

Supplementary Information: Bayesian Optimization and Prediction of the Durability of Triple-Halide Perovskite Thin Films under Light and Heat Stressors

Deniz N. Cakan,^a Eric Oberholtz,^a Ken Kaushal,^a Sean P. Dunfield,^a and David P. Fenning^a

Contents

List of Tables

S1	Compositions of endpoint solutions used for interpolation within $FA_{0.78}Cs_{0.22}Pb(I_xBr_yCl_z)_3$.	2
----	--	---

List of Figures

S1	LED spectrum used in durability testing	3
S2	Model comparison	4
S3	X-ray-diffraction and scanning electron microscopy	5
S4	Voltage deficit of $FA_{0.78}Cs_{0.22}Pb(I_xBr_yCl_z)_3$ films	6
S5	PLQY of $FA_{0.78}Cs_{0.22}Pb(I_xBr_yCl_z)_3$ films	7
S6	Devices from initial search	8
S7	Pearson's correlation matrix of half-cells	9
S8	Raw feature values	10
S9	Histogram of coefficient of variation RMSE	11
S10	Best performing RFR	12
S11	Pearson's correlation matrix of films	13
S12	RFR learning curves	14

^{0a} Aiiso Yufeng Li Family Department of Chemical and Nano Engineering, University of California San Diego, La Jolla, CA, 92093, USA; E-mail: dfenning@ucsd.edu

Table S1 Compositions of endpoint solutions used for interpolation within $FA_{0.78}Cs_{0.22}Pb(I_xBr_yCl_z)_3$.

I_x	Br_y	Cl_z
0.95	0.05	0
0.95	0	0.05
0.80	0.20	0
0.80	0.15	0.05

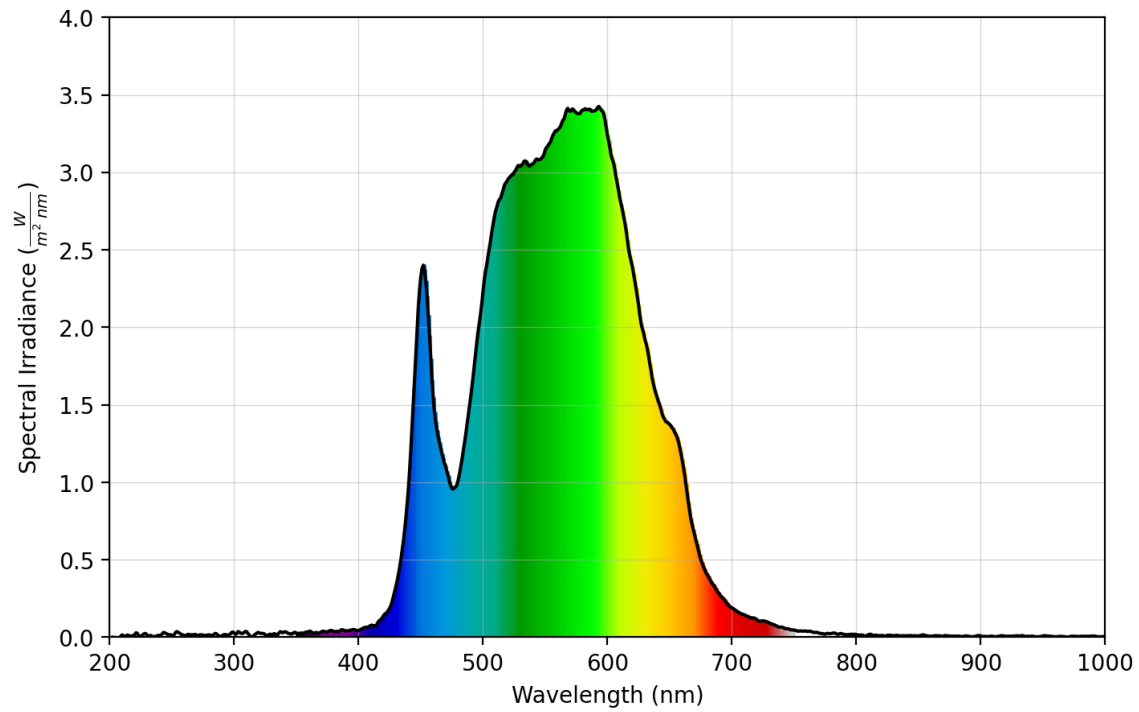


Figure S1 LED spectrum used for the 1-sun test.

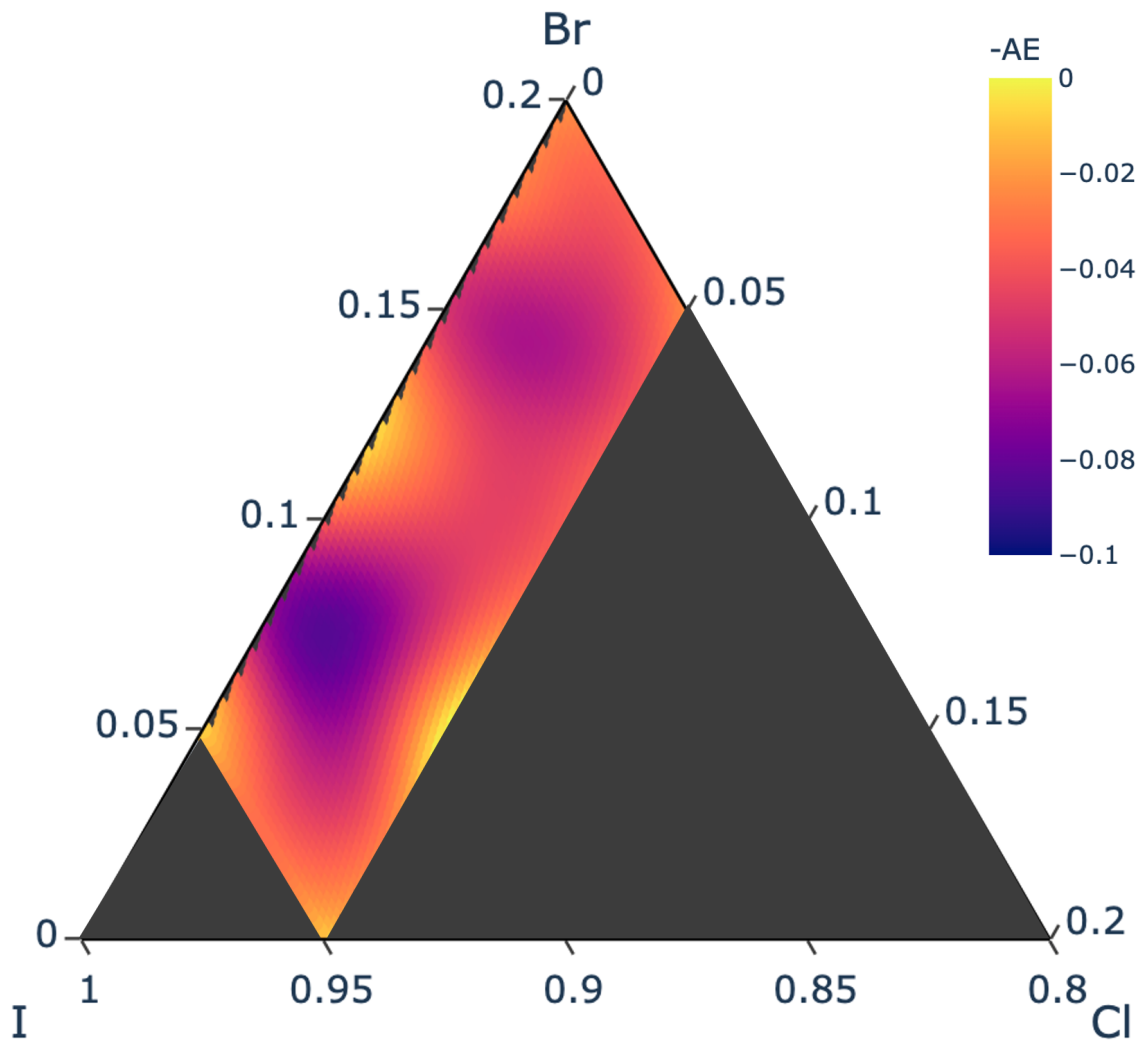


Figure S2 GPR negative absolute error comparison between model produced by samples produced via grid search vs samples produced in BO with EI at 100% exploitation. Color bar yellow depicts regions of relatively minimal difference.

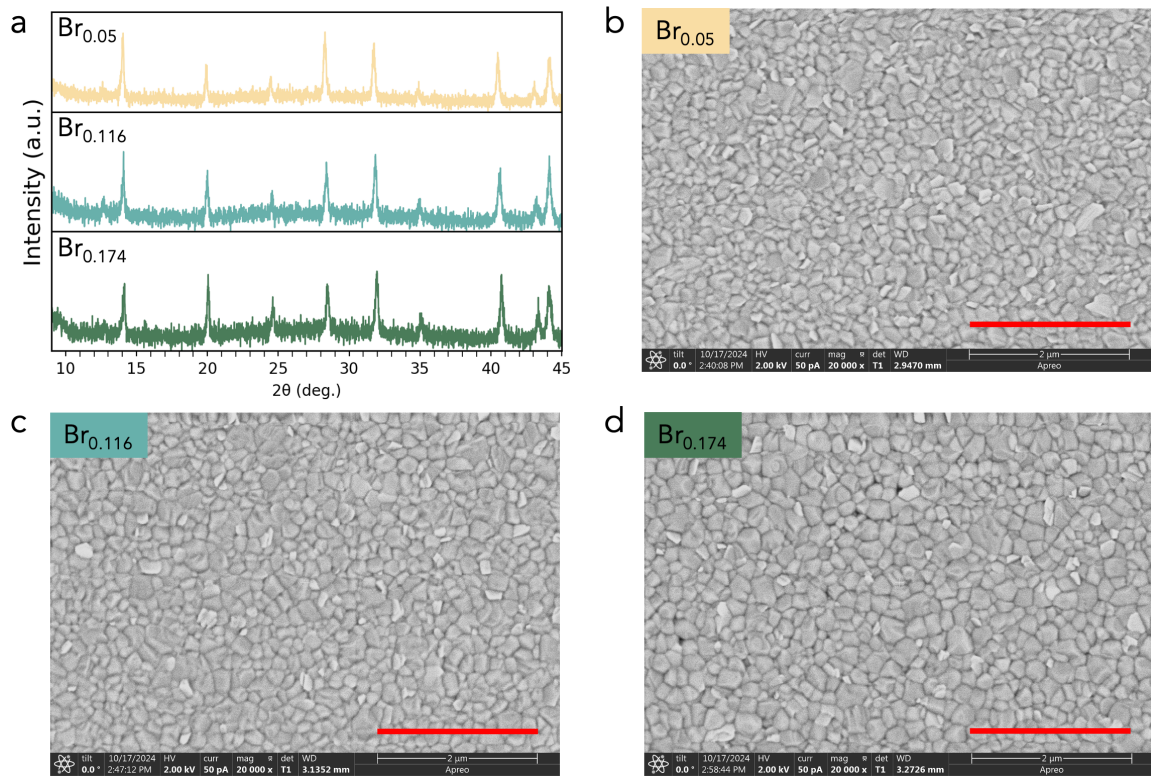


Figure S3 a) XRD and b-d) SEM of $\text{FA}_{0.78}\text{Cs}_{0.22}\text{Pb}(\text{I}_x\text{Br}_y\text{Cl}_z)_3$ films, label inset with Br fraction. Scale bar 2 μm .

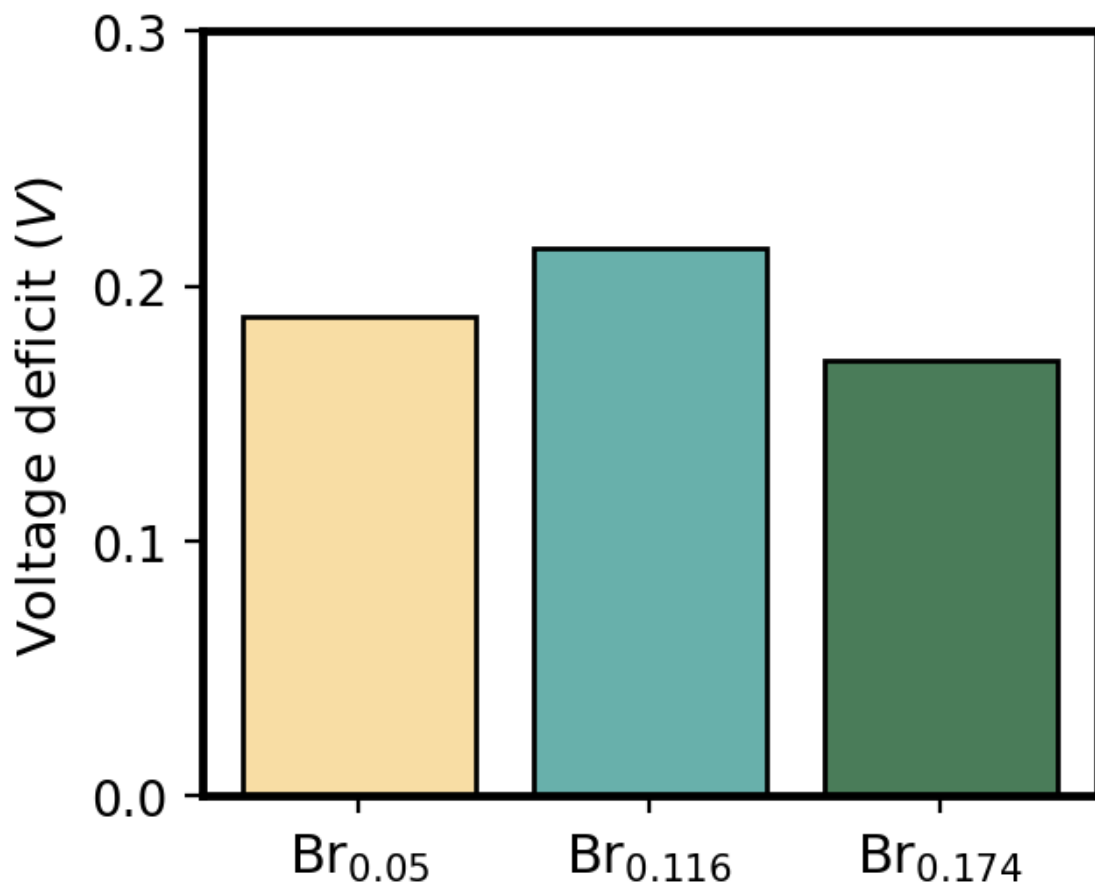


Figure S4 Voltage deficit of $FA_{0.78}Cs_{0.22}Pb(I_xBr_yCl_z)_3$ films.

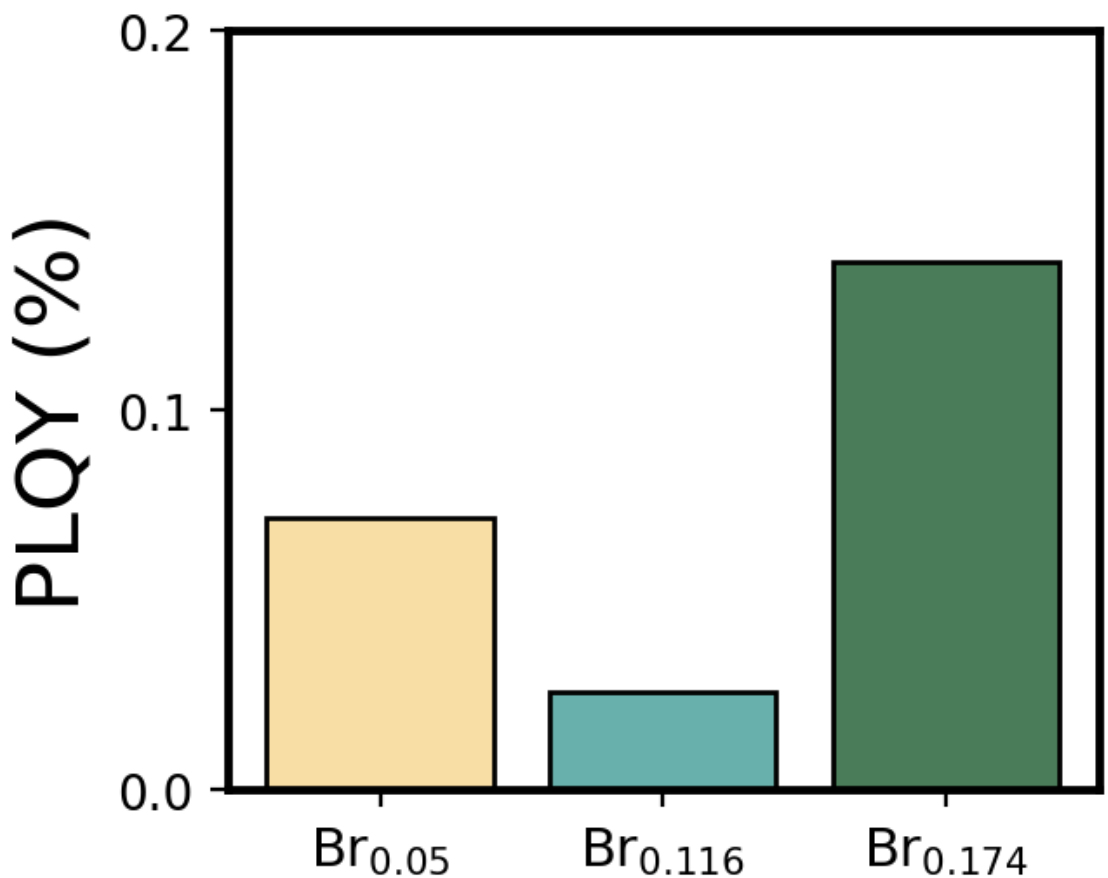


Figure S5 PLQY of $FA_{0.78}Cs_{0.22}Pb(I_xBr_yCl_z)_3$ films.

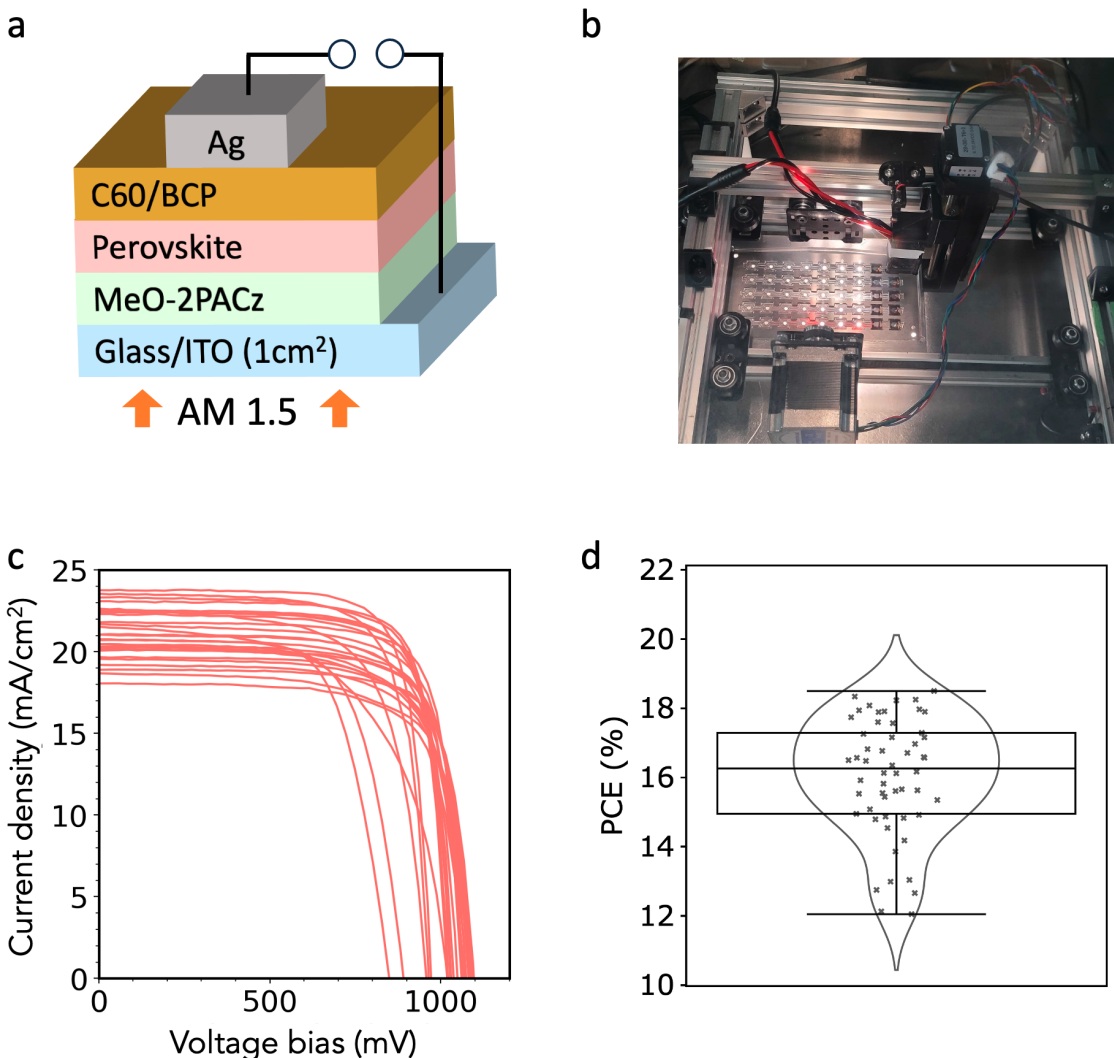


Figure S6 Devices from initial search containing 15 composition unique $FA_{0.78}Cs_{0.22}Pb(I_xBr_yCl_z)_3$ films. a) Schematic of device architecture used in this experiment. b) Photograph of completed 1cm^2 devices in the automatic JV tester system. c) JV curves of the 15 unique samples (3 repeats). d) Box plot with overlaid violin plot of the PCE distribution.

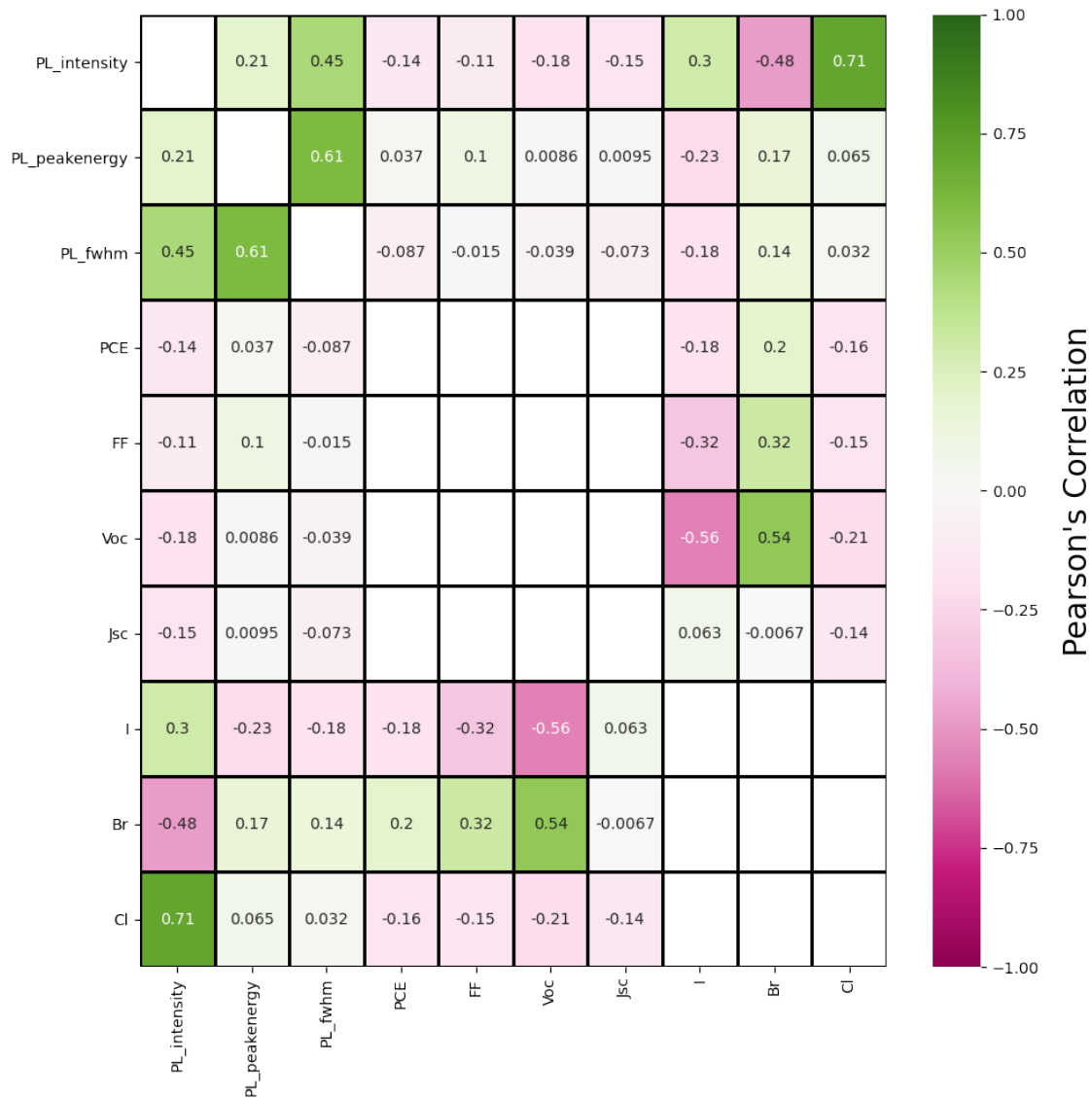


Figure S7 Calculated Pearson's correlation matrix between PL shift, FWHM, and intensity of PL spectra alongside device efficiency (PCE), fill factor (FF), open-circuit voltage (Voc), and short-circuit current density (Jsc) among ITO/MeO-2PACz/PSK/C60/BCP/Ag devices across the PSK compositional space.

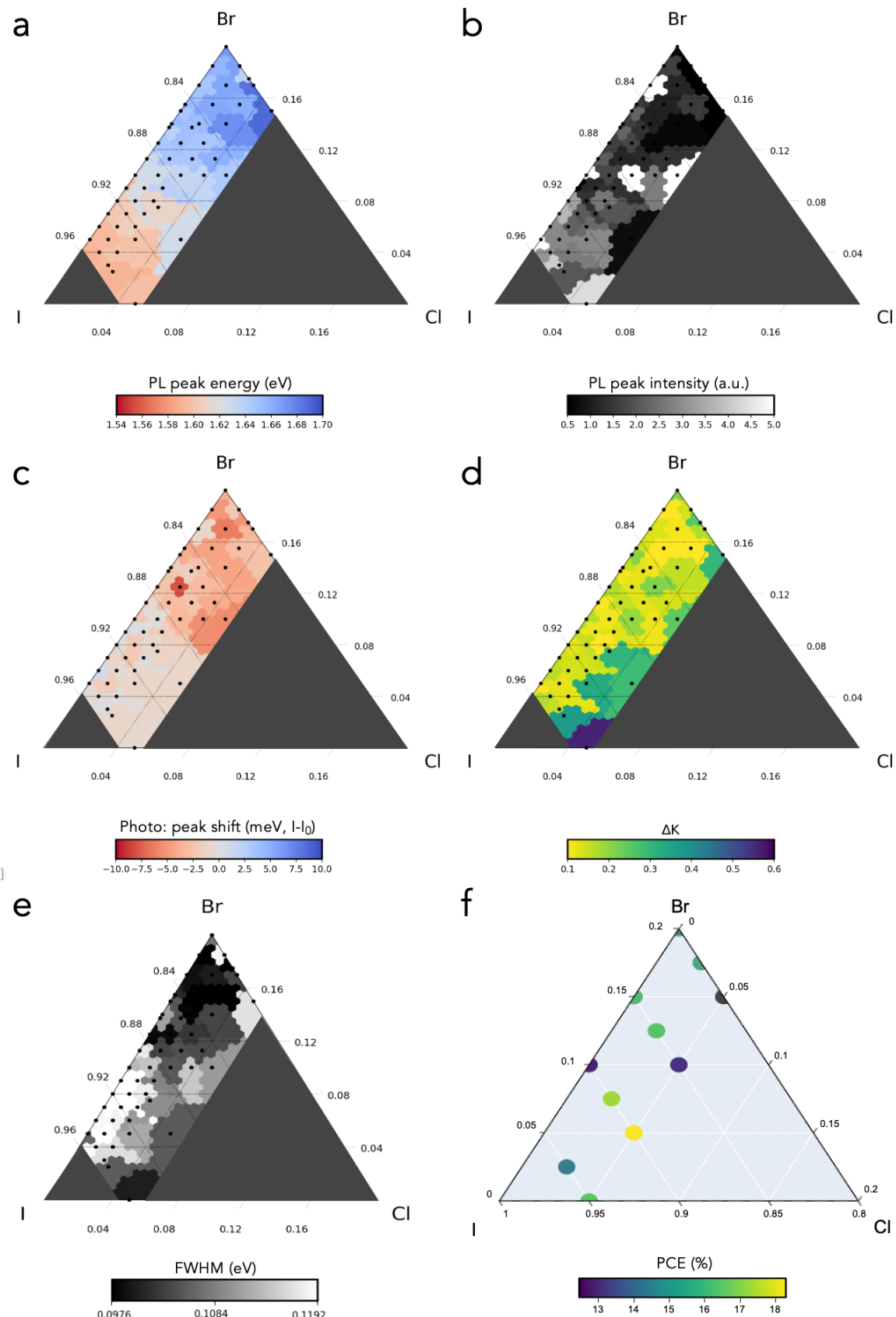


Figure S8 Raw values for characterization used in RFR model training. a) PL peak energy. b) PL peak intensity. c) Photodegradation PL peak shift. d) ΔK extracted from ISOS-L2 testing. Regions of no experiment is shaded out. Color bar located below ternaries. e) PL full-width half max. f) Reverse scan PCE of half-cells.

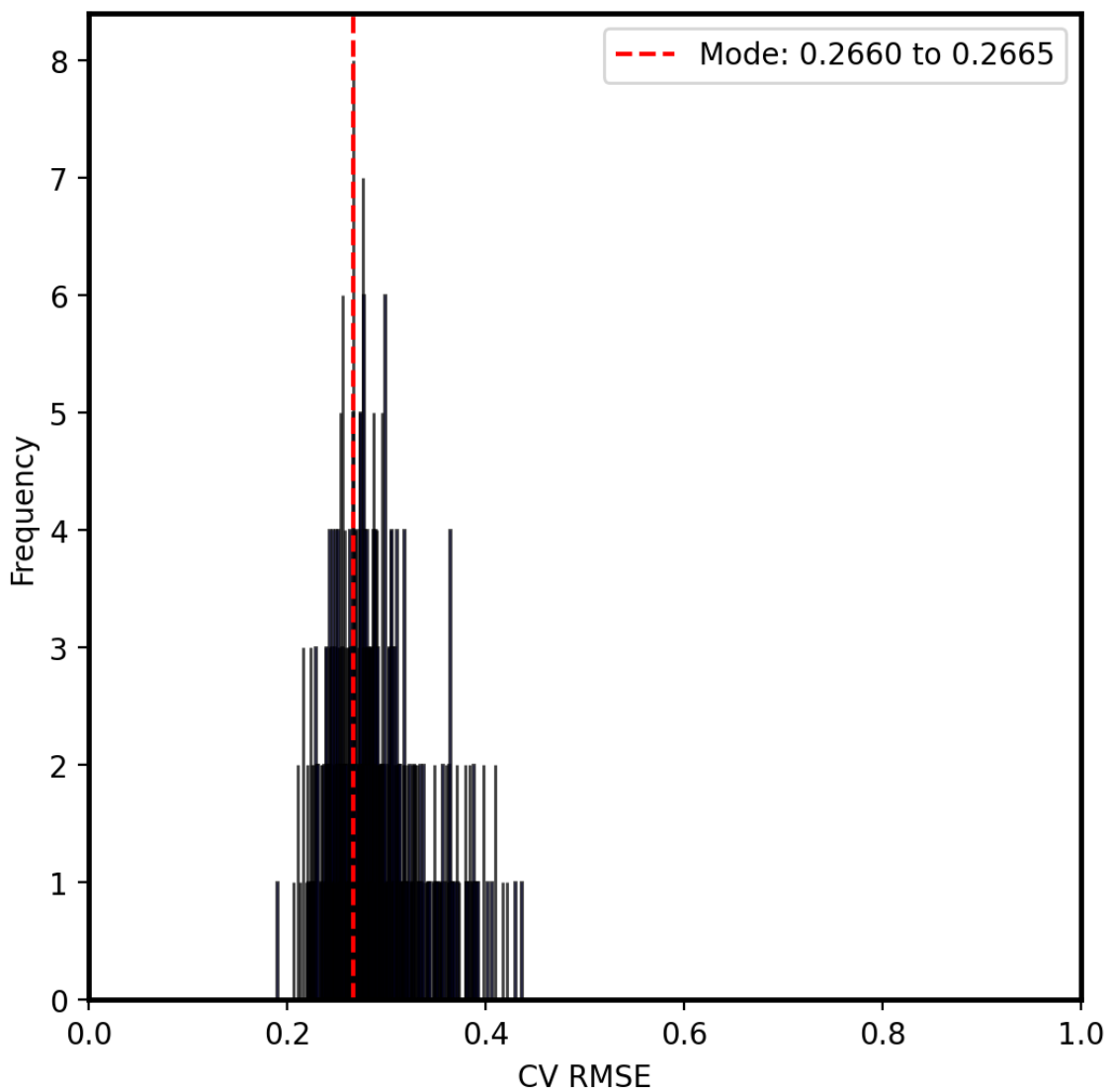


Figure S9 Histogram of coefficient of variation RMSE.

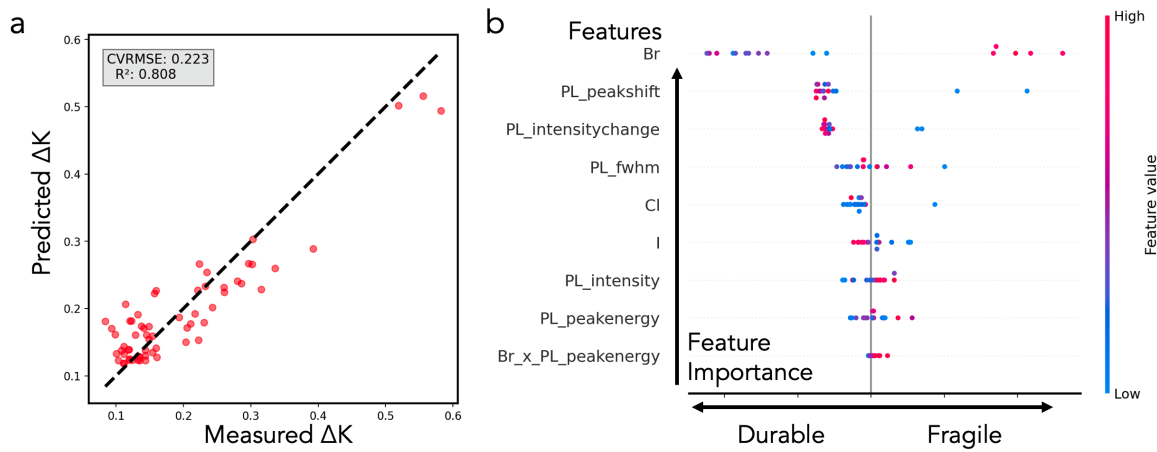


Figure S10 a) Best RFR parity plot and b) corresponding Shap table.

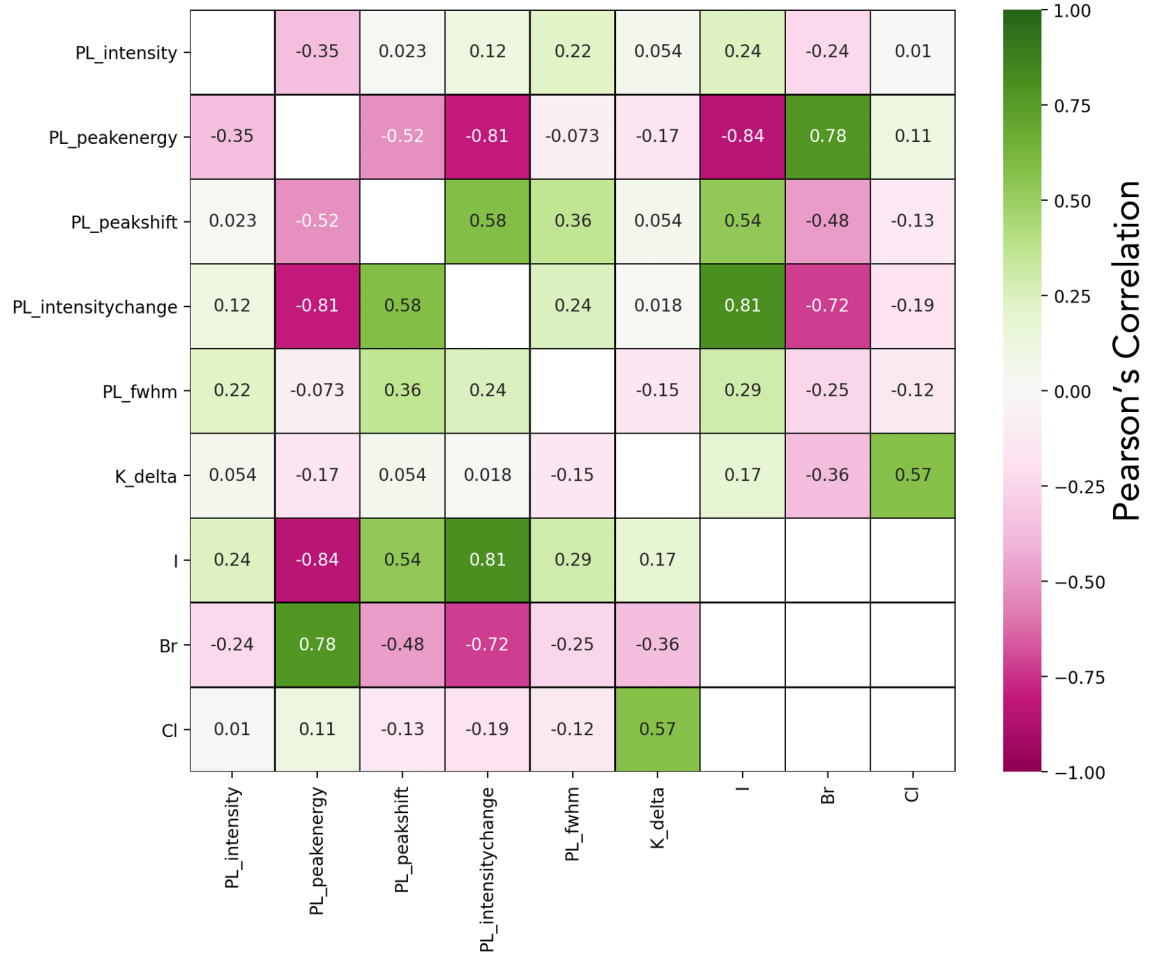


Figure S11 Calculated Pearson's correlation matrix between input variables used in the random forest regression.

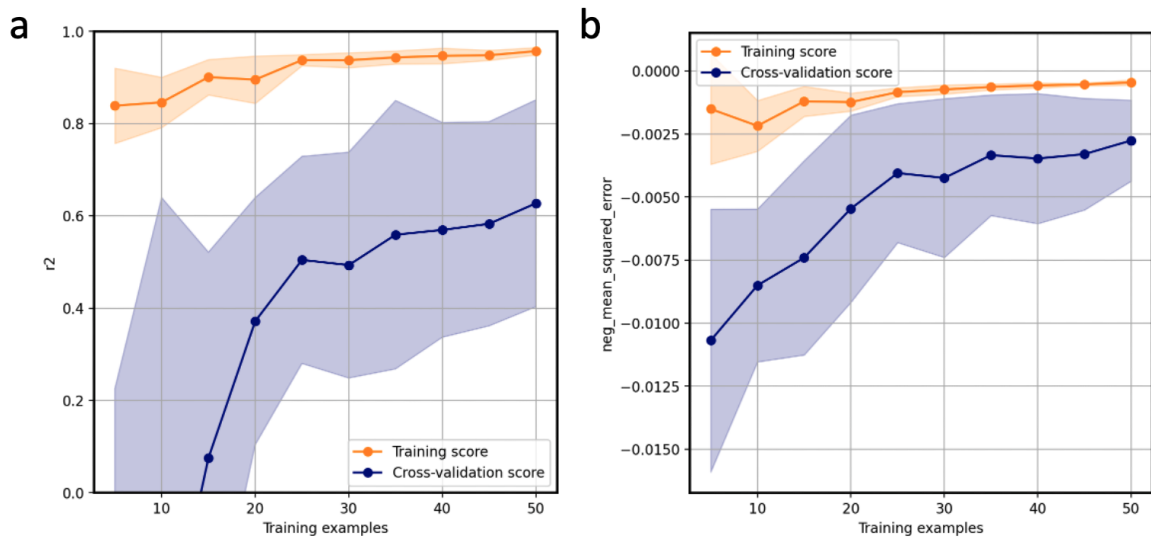


Figure S12 Learning curves showing model's a) R^2 and b) $-\text{MSE}$, as a function of training size.